Fizika Nizkikh Temperatur, 2006, v. 32, No. 2, p. 190–200

# Comparison of pressure, magnetic field and excess manganese effects on transport properties of film and bulk ceramic La–Ca manganites

V.I. Mikhaylov[1], V.P. Dyakonov[1,2], E.E. Zubov[1], A.V. Pashchenko[1], V.N. Varyukhin[1], V.A. Shtaba[1], A. Szewczyk[2], A. Abal'oshev[2], K. Piotrowski[2], K. Dyakonov[3], S.J. Lewandowski[2], and H. Szymczak[2]

[1]*A. Galkin Donetsk Physical-Technical Institute, National Academy of Sciences of Ukraine*
*72 R. Luxemburg Str., Donetsk, 83114, Ukraine*
E-mail: dyakon@dyakon.fti.ac.donetsk.ua

[2]*Institute of Physics, PAS, 32/46 Lotnikow Al., 02- 669 Warsaw, Poland*

[3]*A.F. Ioffe Physical-Technical Institute, RAS, 26 Politechnicheskaya Str., St. Petersburg, 194021, Russia*

Received May 30, 2005, revised August 9, 2005

The pressure, magnetic field and excess manganese effects on transport and magnetoresistance effect (MRE) have been studied in both the epitaxial films and bulk ceramics of manganites $(La_{0.7}Ca_{0.3})_{1-x}Mn_{1+x}O_{3-y}$ ($x$ = 0–0.2). A comparison of electrical behavior in both kinds of samples of similar composition at hydrostatic pressures of up to 1.8 GPa and in a magnetic fields of up to 8 kOe has been performed. The pressure and magnetic field effects are shown to increase with increasing manganese content. Experimental data show that the pressure and magnetic field effects on temperatures of both metal–insulator transition ($T_{MD}$) and MRE peak ($T_{MR}$) are considerably stronger in the films than in ceramics. The hydrostatic pressure increases $T_{MD}$ and $T_{MR}$. Magnetoresistance effect for both types of samples was shown to be favored by the pressure and magnetic field in an opposite way. A direct correlation is established between $T_{MD}$ and conductivity bandwidth as well as between MRE and concentration of charge carriers at applied pressure. The differences in the values of pressure effect on resistance, MRE and $T_{MD}$ temperature in the films and ceramics are connected with both granular structure of ceramics and the oxygen nonstoichiometry in ceramic and film samples of the same content as well as with the film strain induced by lattice mismatch between the film and the substrate. The origin of pressure–magnetic field effects is analyzed in the framework of double exchange interaction and small polaron hopping, and variable range hopping models.

PACS: 72.10.Di, 72.15.Gd, **72.60.+g**, **73.61.–r**, 75.30.Vn, **62.50.+p**

**Keywords**: manganites, resistance, MRE, metal–insulator phase transition, excess manganese, ceramic, double exchange, small polaron hopping and variable range hopping models

## Introduction

The hole-doped manganites, owing to the colossal magnetoresistance effect (MRE) [1,2], are intensively studied functional materials because of both scientific interest and their potential application. The properties of the lanthanum – manganese oxides are controlled by the superexchange and double-exchange (DE) mechanism [3,4]. The superexchange dominates in the compounds containing solely $Mn^{3+}$ or $Mn^{4+}$, leading to antiferromagnetic (AFM) structures. The presence of $Mn^{4+}$ is recognized as necessary for the metallic character found in these compounds when ferromagnetic. The standard methods used to produce a mixture of the $Mn^{3+}$ and $Mn^{4+}$ ionic states involves substituting $La^{3+}$ by Ca, Sr or creating vacancies in the La, Mn, or O sites in $LaMnO_3$. As a result, long-range ferromagnetic order, a metal–insulator transition, and

MRE are induced. A search for a new method of changing $Mn^{4+}$ content is of interest. Therefore in this paper, to change the $Mn^{4+}/Mn^{3+}$ ratio while keeping the La/Ca ratio constant, the method connected with excess manganese doping was used. Unlike the substitution of Ni, Cr, Fe metal ions for Mn ones, which weakens the exchange interactions, the excess Mn doping enhances both magnetic and transport properties of manganites.

Physical properties of magnetoresistive manganites are very sensitive to external perturbations. One of perspective directions for elucidating the nature of the unique interrelation of electrical and magnetic properties and MRE in such manganites is the study of these properties under pressure and in a magnetic field, or with a combination of both. The applied pressure regulating the number of charge carriers at fixed chemical composition allows one to control the electrical and elastic properties of manganites. There are works devoted to research of influence of both pressure (pressure effect) and magnetic field (magnetic-field effect) on magnetic and transport properties of $Ln_{1-x}A_xMnO_3$ (where Ln and A are the rare-earth and alkaline-earth elements, respectively) [5–23]. It could be seen that the pressure – magnetic-field effects on these properties depend strongly on sample morphology: powders, films and single crystals, as well as on grain boundaries, oxygen content, disorder and lattice strain. The literature on pressure and magnetic field effects in La–Ca deals mostly with ceramics [5–15]. Information on the pressure- and magnetic-field-induced changes in the transport properties of $La_{1-x}Ca_xMnO_3$ single crystals [16–19] and films [20–23] is scarce.

A strong influence of manganese excess on magnetic properties and resonance has been established both in La–Ca manganites [24–27] and in self-doping manganites [28]. The main results of the cited references are as follows: using the NMR method it was shown that the manganese ions with ionization states both close to (3+) and (4+) and with intermediate valence result from the high-frequency electron exchange; FM-to-canted spin state transition in clusters of multivalent Mn ions by magnetic and neutron measurements was observed; observation of FMR and spin-wave resonance in the films of manganites with manganese excess.

This work is a continuation of these earlier studies of manganites with excess manganese, and it is focused on the investigation of resistive properties in La–Ca manganites with the general formula $(La_{0.7}Ca_{0.3})_{1-x}Mn_{1+x}O_{3-y}$ ($x$ = 0–0.2). X-ray diffraction and magnetization measurements have been also performed to characterize the samples.

Preliminary studies of the pressure and magnetic-field effects on resistance and magnetoresistance have been performed on film and ceramic samples of manganite with standard composition $La_{0.7}Ca_{0.3}MnO_3$ [23]. However, in Ref. 23, the experimental data on the $\rho(T,P,H)$ dependences were presented without any analysis.

One of the problems studied in this work is the influence of superstoichiometric manganese on conductivity and its role in the magnetoresistive effect. The observed magnetoresistive effect, especially in the films, is shown to increase strongly with increasing content of superstoichiometric manganese.

We also investigated pressure and magnetic-field effects on transport and MRE in the films and ceramics of identical composition varying excess manganese content. It should be noted that the transport measurements were performed under pressure up to 1.8 GPa. In previous studies of pressure and magnetic-field effects in La–Ca manganites [5–22], the following important results have been obtained. Application of pressure was shown to enhance the double-exchange interaction and to enlarge the temperature range of the existence of ferromagnetic phase. A strong electron – phonon interaction arising from the Jahn – Teller splitting of the Mn $d$ levels was also shown to play important role in these materials, since the $e_g$ electrons are involved in the chemical bond formation. The pressure coefficient, $dT_C/dP$, was observed to depend on hole concentration (or the degree of band filling) and to decrease significantly with the hole-doping level. Various structural phases in a number of manganites were induced by hydrostatic pressure. Magnetic-field-induced insulator-to-metal phase transition was also observed in perovskite manganites. The films have shown a more complicated pressure behavior related to the epitaxial stress arising from the lattice mismatch between the film and the substrate, as well as involving the film thickness. Moreover, in the cited works, comparison of pressure and magnetic-field effects on the transport properties of manganites having identical initial composition but different morphology is lacking.

The main result of this paper is the detailed comparison of pressure and magnetic-field effects on conductivity and MRE in ceramic and film samples of manganites with various contents of superstoichiometric manganese (single crystals with the studied compositions were not available) and qualitative analysis of mechanisms responsible for both effects. The influence of pressure and magnetic field on both resistance and the metal–insulator transition temperature in ceramics and the films is similar, but differs in magnitude. The mechanisms responsible for pressure and

magnetic-field effects are also different. The pressure and magnetic-field effects on MRE are shown to have opposite signs. The pressure and magnetic-field effects are analyzed in the frame of double exchange interaction, as well as using small polaron hopping and variable range hopping models.

The studies carried out simultaneously on the films and bulk targets used for their deposition under pressure and in a magnetic field allow to obtain additional information on the transport properties of doped manganites. Among the important new results is the calculation of both the concentration of free charge carriers $n$ and the electron conductivity bandwidth $W$ as well as their changes under pressure in the films with various manganese content. A comparison of the calculated and experimental data shows that there is a direct correlation between $T_{MD}$ and $W$ as well as between MRE and $n$.

## 2. Samples and experimental

The transport properties of $(La_{0.7}Ca_{0.3})_{1-x}Mn_{1+x}O_{3-y}$ manganites with excess manganese were studied in two kinds of samples: ceramics and films. Since the properties of sintered perovskites are very sensitive to preparation conditions, all samples were prepared in the same manner in order to have comparable properties. The ceramics was prepared by the double synthesizing annealing (at 900–950 °C) and sintering of the pressed ($P = 0.5$ MPa) samples in air at 1150 °C with subsequent slow cooling [29]. The superstoichiometric (excess) manganese with valencies of $Mn^{3+}$ и $Mn^{4+}$ replace the cation vacancies in octahedral positions of the $B$ sublattice formed as a result of cyclic oxidation – reduction processes occuring during at synthesis and sintering.

Using a ceramic target with diameter of 24 mm, the films of studied compositions were deposited onto $LaSrGaO_4$ substrate having the temperature ~ 800 °C by pulsed laser deposition. The film thickness was about 1000 Å. To optimize the $Mn^3/Mn^{4+}$ ratio, to saturate by oxygen and to improve the homogeneity of the films, the latter were additionally annealed at 600 °C in an oxygen atmosphere.

The specific resistance ρ and magnetoresistance effect $\Delta R/R_0 = (R_0 - R_H)/R_0$, where $R_0$ and $R_H$ are the resistance in zero and $H$ magnetic fields, respectively, as a function of both pressure (up to 1.8 GPa) and magnetic field ($H = 0$–8 kOe) were measured using the conventional dc four-probe method in the temperature interval of 4.2–300 K.

The hydrostatic pressure was produced in a two-layer chamber made from nonmagnetic steel (a channel is 6.5 mm in diameter and external diameter of chamber is 30 mm). A mixture of mineral oil and kerosene was used as a pressure transmitting medium. At high temperatures, the pressure and temperature were measured *in situ* by manganin and copper wire gauges located next to the sample. At low temperatures, the pressure was determined using the pressure dependence of superconducting transition temperature of a Sn probe.

## 3. Experimental results

According to room temperature x-ray diffraction data, the ceramic samples are single-phase with no other detectable phases and have the perovskite structure (*Pnma*). The films are also single-phase, epitaxial and oriented along the pseudo-cubic axis [100]. Both in ceramics and films, the Mn doping does not change the structural symmetry and leads to a decrease of the cell parameters (Table 1). The decrease of the unit cell volume can be attributed to both the reduction of $Mn^{3+}$ to $Mn^{4+}$, with smaller ionic radii and the creation of vacancies.

As is seen from Table 1, the lattice parameters and phase transitions temperatures in ceramic and film samples of the same composition are different. This is due to the difference in oxygen stoichiometry. The oxygen deficiency (oxygen nonstoichiometry) in the films is confirmed by both lower phase transitions temperatures and quasi-cubic structure. It is observed in the majority of works dealing with the properties of manganites as a function of oxygen content [30–33].

Table 1. Crystal structure parameters, Curie temperature $T_C$, metal–insulator transition $T_{MD}$ and MRE peak ($T_{MR}$) temperatures (at $P = 0$ and $H = 0$) and $\Delta R/R$ value ($H = 8$ kOe).

| Parameters of cell | | | | $T_C$, K | $T_{MD}$, K | $T_{MR}$, K | $\Delta R/R$, % |
|---|---|---|---|---|---|---|---|
| $x$ | $a$, Å | $b$, Å | $c$, Å | | | | |
| ceramics | | | | | | | |
| LCMO | 5.505 | 5.552 | 7.796 | 265 | 277 | 276 | 14 |
| LCM1O | 5.464 | 5.515 | 7.728 | 267 | 272 | 269 | 20 |
| LCM2O | 5.458 | 5.464 | 7.718 | 270 | 273 | 270 | 22 |
| films | | | | | | | |
| LCMO | 3.890 | – | – | 210 | 238 | 215 | 20 |
| LCM1O | 3.868 | – | – | 222 | 267 | 248 | 33 |
| LCM2O | 3.866 | – | – | 225 | 270 | 249 | 50 |

The temperature dependences of resistance ρ and magnetoresistance $\Delta R/R_0$ in manganites with different manganese content [$La_{0.7}Ca_{0.3}MnO_{3-y}$ (LCMO), $(La_{0.7}Ca_{0.3})_{0.9}Mn_{1.1}O_{3-y}$ (LCM1O), and $(La_{0.7}Ca_{0.3})_{0.8}Mn_{1.2}O_{3-y}$ (LCM2O)] measured at zero and high pressure, with and without magnetic field, are illustrated in Fig. 1 (for ceramics) and Fig. 2

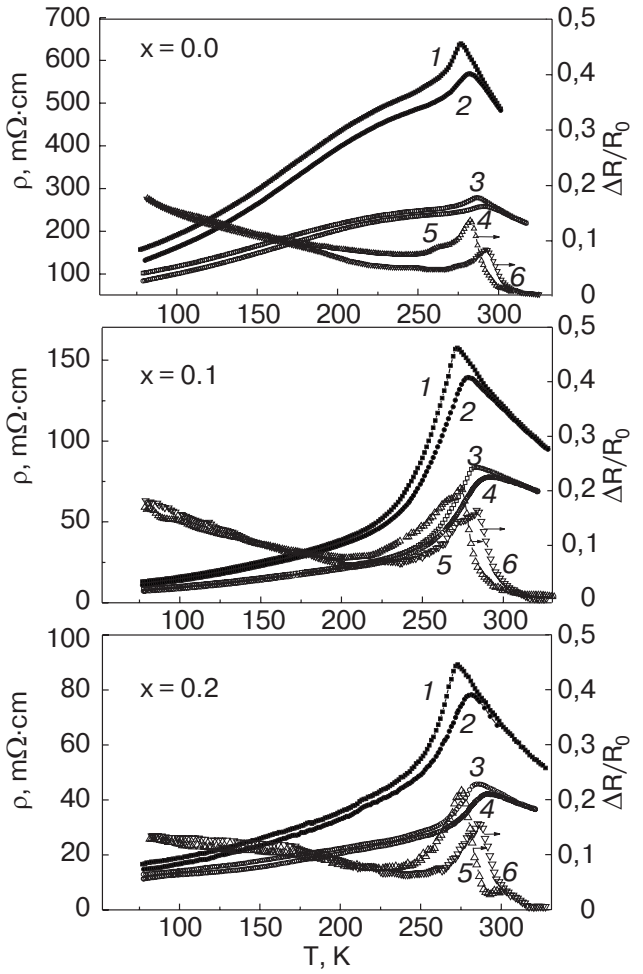


*Fig. 1.* Temperature dependence of specific resistance ρ (curves *1–4*) and magnetoresistance effect, $\Delta R/R_0$, (curves *5–6*) in the ceramic samples $(La_{0.7}Ca_{0.3})_{1-x}Mn_{1+x}O_3$ at different manganese content, pressure (GPa) and applied magnetic field (kOe): *1* — $P = 0$, $H = 0$; *2* — $P = 0$, $H = = 8.0$; *3* — $P = 1.8$, $H = 0$; *4* — $P = 1.8$, $H = 8.0$; *5* — $P = 0$, $H = 8.0$; *6* — $P = 1.8$, $H = 8.0$.

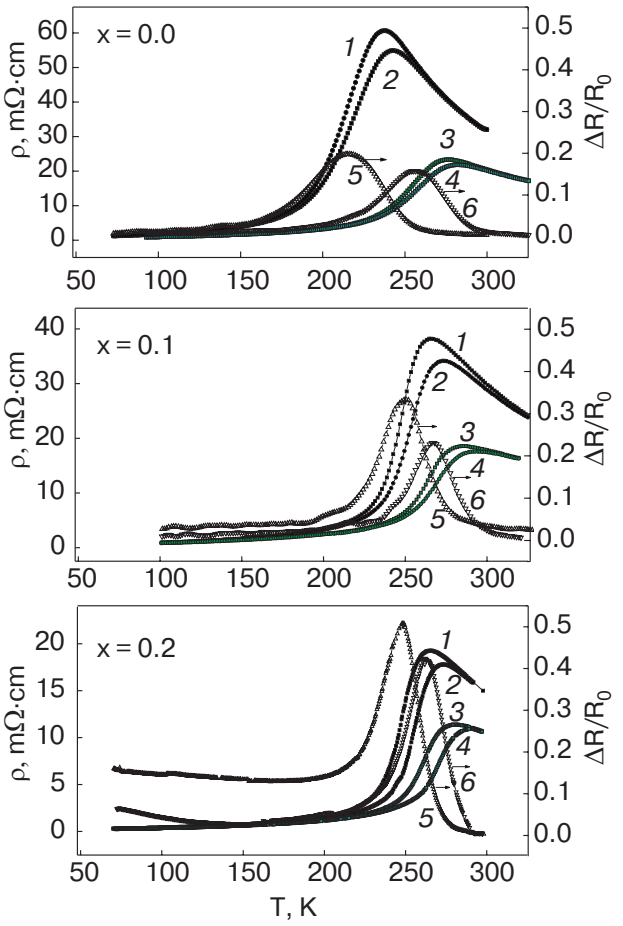


*Fig. 2.* Thermal dependence of specific resistance ρ (curves *1–4*) and magnetoresistance effect, $\Delta R/R_0$, (curves *5–6*) in the film samples $(La_{0.7}Ca_{0.3})_{1-x}Mn_{1+x}O_3$ at different manganese content, pressure (GPa) and applied magnetic field (kOe) : *1* — $P = 0$, $H = 0$; *2* — $P = 0$, $H = 8.0$; *3* — $P = 1.8$, $H = 0$; *4* — $P = 1.8$, $H = 8.0$; *5* — $P = 0$, $H = 8.0$; *6* — $P = 1.8$, $H = 8.0$.

(for films). The $\rho(T)$ curves for the intermediate values of pressure and magnetic field are not shown so as not to obscure the figures. A characteristic phase transition temperatures and MRE values in ceramic and film samples and their changes under pressure are summarized in Tables 1–3.

From Figs. 1 and 2 it is seen that the maximum of resistance in both ceramics and the films decreases as a manganese content increases. The low values of room temperature and the residual resistances and the sharp decrease of the $\rho(T, P)$ peak below $T_{MD}$ in the films in comparison with the ceramics indicate the absence of significant grain boundary contributions to the resistivity. The temperature coefficient of resistance changes from negative to positive upon cooling through the peak resistance temperature, $T_{MD}$, corresponding to a metal–insulator transition. The $T_{MD}$ in the films is appreciably less than in the ceramics and increases with increasing $x$. The decrease of maximum resistance and the increase of $T_{MD}$ with increasing manganese content are attributed to the increase of charge carriers as a result of the increase of the $Mn^{4+}/Mn^{3+}$ ratio. The difference of both resistance and $T_{MD}$ in ceramics as compared to ρ and $T_{MD}$ in the films of the same composition is assumed to result from both structural irregularities in ceramics and the film strain induced by lattice mismatch between the film and the substrate. The resistance is higher in ceramics than in the films because of the differences in oxygen stoichiometry in the two types of samples. The additional scattering of charge carriers from defects and grain boundaries in ceramics also leads to a reduction in intergranular conductivity. These data correlate with a previous reports [30–33]. Using the data on the in-

terrelation between the phase transition temperature and oxygen nonstoichiometry ($\Delta y$) [33], the difference in oxygen nonstoichiometry for the ceramics ($c$) and the films ($f$) studied was estimated. Knowing $\Delta T_{MD} = T_{MD}^{f} - T_{MD}^{c}$, we have $\Delta y \approx 1.6 \cdot 10^{-1}$ and $3 \cdot 10^{-2}$ in LCMO and LCM2O, respectively. A decrease of $\Delta y$ in LCM2O correlates with the fact that the $T_{MD}$ temperatures for ceramics and the films come close together as $x$ increases from 0 to 0.2.

Table 2. Curie temperature ($T_C$), metal–insulator transition ($T_{MD}$) and MRE peak ($T_{MR}$) temperatures, $\Delta R/R_0$ value (in magnetic field of 8 κOe) at pressures mentioned in text and pressure coefficients $dT_C/dP$ and $dT_{MR}/dP$.

| Samples | $T_C$, K | $T_{MD}$, K | $T_{MR}$, K | $\frac{dT_C}{dP}$, K/GPa | $\frac{dT_{MR}}{dP}$, K/GPa | $\frac{\Delta R}{R_0}$, % |
|---|---|---|---|---|---|---|
| ceramics | | | | | | |
| LCMO | 275 | 286 | 285 | 10.5 | 5.0 | 8 |
| LCM1O | 279 | 283 | 279 | 11.5 | 5.5 | 16 |
| LCM2O | 280 | 285 | 281 | 13.8 | 6.0 | 16 |
| films | | | | | | |
| LCMO | – | 276 | 256 | – | 23 | 16 |
| LCM1O | – | 286 | 267 | – | 11 | 23 |
| LCM2O ($P$ = 0.9 GPa) | – | 281 | 262 | – | 13 | 42 |

Table 3. Metal–insulator transition temperature ($T_{MD}$) and values of $\Delta T_{MD}/\Delta H$ and $dT_{MD}/dP$ at pressure (GPa) in magnetic fields (kOe).

| Samples | $T_{MD}$, ($P$ = 0, $H$ = 8) K | $T_{MD}$, ($P$ = 1.8, $H$ = 8) K | $\frac{\Delta T_{MD}}{\Delta H}$ ($P$ = 0) K/kOe | $\frac{\Delta T_{MD}}{\Delta H}$ ($P$ = 1.8) K/kOe | $\frac{dT_{MD}}{dP}$ ($H$ = 0; 8) K/GPa |
|---|---|---|---|---|---|
| ceramics | | | | | |
| LCMO | 283 | 285 | 10.5 | 5.0 | 8 |
| LCM1O | 281 | 279 | 11.5 | 5.5 | 16 |
| LCM2O | 281 | 281 | 13.8 | 6.0 | 16 |
| films | | | | | |
| LCMO | 243 | 282 | 0.6 | 0.8 | 21 |
| LCM1O | 274 | 294 | 1.1 | 1.0 | 11 |
| LCM2O | 273 | 291 ($P$ = 0.9) | 1.1 | 1.1 ($P$ = 0.9) | 11 |

Since the correlation between the temperature-dependent changes of resistance and magnetization near the phase transition is observed, the semiconducting character of the conductivity in the paramagnetic phase can be interpreted being the result of thermal spin fluctuations and the resultant spatial randomness of the transfer interaction. At $T > T_{MD}$ one observes activated behavior of the resistance, and hopping conductivity is the dominant conduction mechanism. Due to the closeness of $T_{MD}$ to room temperature there are not sufficient data to carry out an exact calculation of the temperature dependence of the resistivity. In an attempt to find the best theoretical fit to the experiment, we have tested each approximation for the minimal root-mean-square deviation (less 0.5%) of experimental and calculated points. The temperature variation of the electrical conductivity in ceramic and film samples above $T_{MD}$ was analyzed using both hopping of small polarons [34–36] and Mott's variable range hopping (VRH) [37] models. The model of small polaron hopping predicts that

$$\rho(T) = \rho_0 T^{\alpha} \exp\left(\frac{E_A}{k_B T}\right), \qquad (1)$$

where $\alpha = 1$ for an adiabatic small polaron hopping model [35] or $\alpha = 1.5$ for nonadiabatic small polaron hopping model [34,36].

Within an alternative VRH model

$$\rho(T) = \rho_0 \exp\left(T_0 / T\right)^{1/4}. \qquad (2)$$

In these formulas, $E_A$ is the activation energy, $\rho_0$ is the residual temperature-independent part of the resistance, $T_0$ is the Mott temperature, and $k_B$ is Boltzmann's constant.

It is important to note that the $\rho(T)$ dependences in ceramics are better fitted by Mott's law (Eq. (2)), while in the films the root-mean-square fitting using the nonadiabatic small polaron hopping model with $\alpha = 1.5$ gives smaller deviations from the experiment. Despite the narrow temperature range of fitting, the data of the analysis correlate with theoretical results [38,39]. The results of the fitting of experimental data for the films are presented in Table 4 for various compounds. The $E_A$ values calculated correlate with ones obtained in work [36]. It should be noted that the activation energy decreases with increasing manganese content.

At $T < T_{MD}$, the resistivity curves show metallic-like behavior. In the framework of the double-exchange model [3,4], where the conduction takes place via hopping of the $e_g$ electrons between two Mn ions, the transfer integral is expressed as $t_{\text{eff}} = t_0 \cos(\theta_{ij}/2)$, where $t_0$ depends on both the Mn–O–Mn bond angle and the Mn–O bond length. The relative angle $\theta_{ij}$ between two neighbouring Mn spins in the $i$ and $j$ sites decreases with diminishing temperature owing to the ferromagnetic alignment of the Mn spins, and as a result $\rho$ will decrease.

In low-temperature region ($T < 0.5T_{MD}$), the experimental data were fitted by the following expres-

Table 4. Resistance ($\rho_0$, $\rho_1$), activation energy ($E_A$) in the films in magnetic field (kOe) and at pressures (GPa).

| | High $T$ | | $H$ = 0 Low $T$ | | High $T$ | | $H$ = 8 Low $T$ | |
|---|---|---|---|---|---|---|---|---|
| | $\rho_0$, mΩ·cm | $E_A$, K | $\rho_0$, mΩ·cm | $\rho_1$, mΩ·cm/K$^{2.5}$ | $\rho_0$, mΩ·cm | $E_A$, K | $\rho_0$, mΩ·cm | $\rho_1$, mΩ·cm/K$^{2.5}$ |
| LCMO $P$ = 0 | $9.5\cdot10^{-5}$ | 1251 | 0.815 | $9.96\cdot10^{-6}$ | $1.03\cdot10^{-4}$ | 1227 | 0.813 | $9.75\cdot10^{-6}$ |
| LCMO $P$ = 1.8 | $1.04\cdot10^{-4}$ | 1089 | 0.555 | $4\cdot10^{-6}$ | $1.13\cdot10^{-4}$ | 1061 | 0.546 | $4\cdot10^{-6}$ |
| LCM1O $P$ = 0 | $1.04\cdot10^{-4}$ | 1205 | 0.463 | $4.32\cdot10^{-6}$ | $1.04\cdot10^{-4}$ | 1105 | 0.402 | $4.4\cdot10^{-6}$ |
| LCM1O $P$ = 1.8 | $2.11\cdot10^{-4}$ | 836 | 0.508 | $3.3\cdot10^{-6}$ | $2.25\cdot10^{-4}$ | 812 | 0.505 | $3.23\cdot10^{-6}$ |
| LCM2O $P$ = 0 | $7.6\cdot10^{-5}$ | 1092 | 0.242 | $1.92\cdot10^{-6}$ | $8.4\cdot10^{-5}$ | 1059 | 0.203 | $1.67\cdot10^{-6}$ |
| LCM2O $P$ = 1.0 | $1.31\cdot10^{-4}$ | 824 | 0.224 | $1.55\cdot10^{-6}$ | $1.03\cdot10^{-4}$ | 894 | 0.201 | $1.61\cdot10^{-6}$ |

sions: a) $\rho(T) = \rho_0 + \rho_1 T^2$ (one-magnon contribution to resistivity) [40,41] and b) the empirical relation $\rho(T) = \rho_0 + \rho_1 T^{2.5}$ [6,42].

For ceramics the one-magnon contribution to resistivity is prevalent as shown in Fig. 3 for LCMO, LCM1O, and LCM2O.

The law $\rho(T) = \rho_0 + \rho_1 T^{2.5}$ has the smallest roughness and is more suitable for fitting of $\rho(T)$ in the films. In Fig. 4, the low-temperature dependence of the resistance is presented as a function of $T^{2.5}$ for the LCMO, LCM1O, and LCM2O films.

The following data demonstrate the high sensitivity of transport properties of manganites to the external pressure (Figs. 1 and 2; Tables 2–4). The $\rho(T, P)$ dependences show reversible behavior near the phase transition. For all samples, the pressure results in increasing electrical conductivity in the whole temperature range. Near room temperature $\rho$ decreases at a rate of ~ − (35–48) %/GPa, depending on $x$. Near $T_{MD}$ the sensitivity of the resistance to pressure is particularly enhanced, and the maximum derivative $d\rho/dP$ is observed. The pressure dependence of resistance is practically linear up to 1.5 GPa for both types of samples, allowing the use of manganite as a pressure sensor. These dependences have a form: $\rho^c(P) \sim 490 - 134P$ and $\rho^f(P) \sim 30 - 5.5P$ for the LCMO ceramics and film, respectively, and $\rho^c(P) \sim 67 - 14P$ and $\rho^f(P) \sim 15 - 4P$ for the LCM2O ceramics and film, respectively, at room temperature, where $\rho$ (mΩ·cm) and $P$ (GPa).

At $T > T_{MD}$, Mott's law is rather well followed in ceramics under pressure over a temperature range. The characteristic Mott's temperature obtained from fitting procedures is comparable to values reported for other doped manganites. The value of $T_0$ is established to decrease with increasing pressure. As an illustration, the $T_0(P)$ dependence for LCM1O is presented in the inset of Fig. 3. As seen in Table 4, the activation energy is lowered by external pressure, that is indicative of reduction in the energy of electron localization. $E_A$ is shown to be also less in the films with a higher $T_{MD}$.

At temperatures below $T_{MD}$ the ferromagnetic domains form percolating conducting paths. The strength of the percolation increases with increasing pressure as the volume of FM phase increases. The low-temperature $\rho(T)$ dependence in ceramics under pressure has been well fitted to the expression $\rho_0(T) = \rho_0(0) + \rho_1 T^2$ (Fig. 3). In Fig. 4 the low-temperature resistances as a function of $T^{2.5}$ for the film samples are shown at different pressures. The tangent of the slope of the curves is shown to decrease under

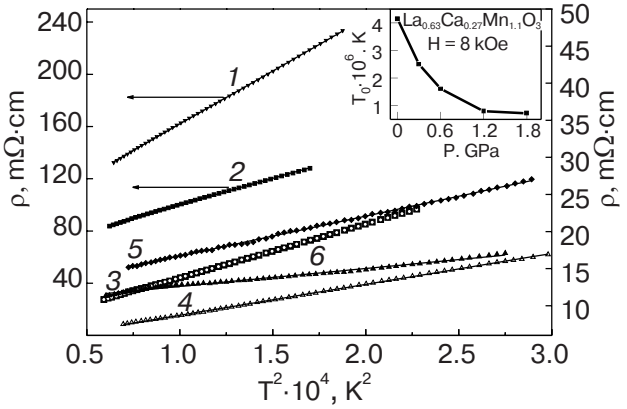


*Fig. 3.* Fits of the low temperature dependence of resistance $\rho(T)$ in ceramics with different manganese content to the expression $\rho(T) = \rho_0 + \rho_1 T^2$ under pressure (GPa) in magnetic field $H$ = 8 kOe: LCMO (left ordinate axis), *1* — $P$ = 0, $\rho_0$ = 59.4 mΩ·cm; *2* — $P$ = 1.8, $\rho_0$ = = 59.4 mΩ·cm; LCM1O, *3* — $P$ = 0, $\rho_0$ = 6.6 mΩ·cm; *4* — $P$ = 1.8, $\rho_0$ = 4.5 mΩ·cm and LCM2O, *5* — $P$ = 0, $\rho_0$ = = 11.3 mΩ·cm; *6* — $P$ = 1.8, $\rho_0$ = 10.2 mΩ·cm (right ordinate axis for LCM1O and LCM2O). The inset shows the pressure dependence of Mott temperature in LCM1O ceramics at $T > T_{MD}$.

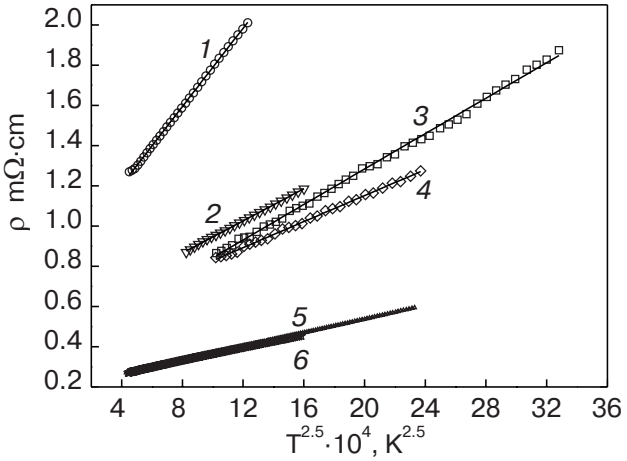


*Fig. 4*. Fits of the low temperature dependence of resistance $\rho(T)$ in the films with different manganese content to the expression $\rho(T) = \rho_0 + \rho_1 T^{2.5}$ under pressure (GPA) in applied magnetic field of 8 kOe: ($x = 0$), 1 — $P = 0$; 2 — $P = 1.8$; ($x = 0.1$), 3 — $P = 0$; 4 — $P = 1.8$ ; ($x = 0.2$) 5 — $P = 0$, 6 — $P = 0.9$. The $\rho_0$ and $\rho_1$ values are shown in Table 4.

pressure in both ceramics and the films. One can see that the pressure effect on $\rho(T)$ decreases with increasing $x$.

The resistance peak temperatures determined on the basis of spline interpolation of $\rho(T)$ experimental points shift towards higher temperatures with increasing pressure. The pressure effect on $T_{MD}$ is stronger in the films than in ceramics. At a pressure of 1.8 GPa ($H = 0$), $T_{MD}$ increases by 9, 11, and 12 K in ceramic LCMO, LCM1O, and LCM2O samples, while in the films of the same composition it increases by 38, 21, and 11 K (0.9 GPa), respectively (Tables 2 and 3).

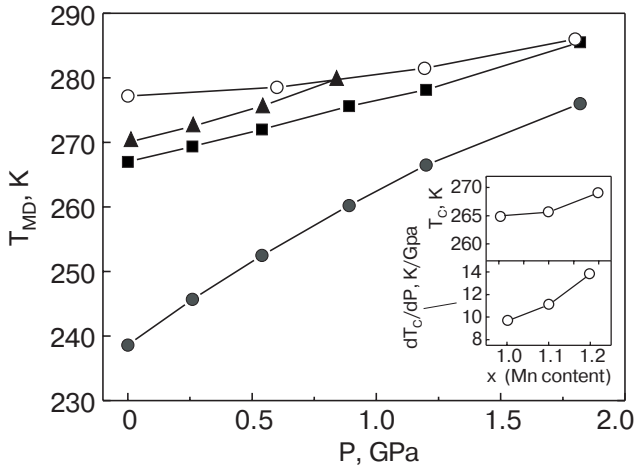


*Fig. 5*. Pressure dependences of $T_{MD}$ in the films with $x = 0$ (full circle); 0.1 (full square) and 0.2 (full triangle) as well as in ceramics with $x = 0$ (open circle). Inset — $dT_C/dP$ and $T_C$ dependences as a function of Mn content in ceramics.

The hydrostatic pressure reduces the distinction of $T_{MD}$ in the films and ceramics. It stems from the fact that pressure not only affects the unit cell parameters but also influences the film microstructure due to epitaxial strain. Owing to this, in the films with low $T_{MD}$ a pressure moves $T_{MD}$ towards a higher temperature at a faster rate compared with the films having a high $T_{MD}$. The $T_{MD}(P)$ dependences for the LCMO, LCM1O, and LCM2O films and LCMO ceramics are presented in Fig. 5. The pressure effect on $T_{MD}$ is positive and has close to linear character up to 1.8 GPa for all samples studied. The pressure coefficient is a convenient criterion for the sensitivity of $T_{MD}$ to pressure. The $dT_{MD}/dP$ derivatives for ceramics are practically Mn doping-independent, while in the films they decrease with Mn content from 21 K/GPa for LCMO to 11 K/GPa for LCM2O (Table 3). Thus, the lowest $dT_{MD}/dP$ value is observed for compounds with the highest $T_{MD}$ (and highest value of $x$) as well as with the highest electrical conductivity. A similar correlation and close values of $dT_{MD}/dP$ were obtained in other parent oxides $La_{1-x}Ca_xMnO_3$. For comparison, in the inset of Fig. 5 the Curie temperature, $T_C$, and pressure coefficient $dT_C/dP$ as a function of Mn concentration obtained as a result of measurements of magnetization under pressure are presented for $x = 0$, 0.1, and 0.2.

In parallel with the pressure effect (at $H = 0$), the magnetic-field effect on magneto-transport properties has been studied, and the comparison of both effects was performed. The field effect on the resistance of both types of samples qualitatively resembles the influence of pressure on $\rho$ (Figs. 1 and 2). An applied magnetic field shifts the $\rho(T)$ peak towards higher temperatures. The magnetic field of 8 kOe increases the conductivity at $T_{MD}$ by about 12%, resulting in CMR effect.

Above $T_{MD}$, the temperature dependence of resistance is fitted to Mott's law (Eq. (2)). A weak field dependence of $T_0$ with magnetic field is observed. As for $\rho(T, P)$ in zero field below $T_{MD}$, the empirical expression $\rho(T) = \rho_0 + \rho_1 T^{\alpha}$ can be used to fit the magnetic field dependence of low-temperature resistance. The best fit was obtained for $\alpha = 2$ and 2.5 for ceramics and the films, respectively. The tangent of slope of the curves $\rho(T, P)$ does not change with magnetic field. According to the data obtained, a magnetic field reduces the activation energy, and, as a consequence, $\rho(T)$ decreases near the metal–insulator transition.

The maximum change of $\Delta R/R_0$ is observed near the phase transition. MRE changes stronger in the film than in ceramics with Mn doping, namely, the $\Delta R/R_0$ value increases by 14 and 22% in a magnetic field of 8 kOe for $x = 0$ and 0.2, respectively, while in

the films of the same compositions, MRE increases from 20 to 50% (Table 1). A smaller $\Delta R/R_0$ value in ceramics than in the films is connected with their granular structure. At low temperatures, MRE increases in ceramics and there is no detectable MRE change in the films.

An application of pressure results in reduction of the negative magnetoresistance peak. The MR effect near $T_{MD}$ is decreased by about 4–10% in samples with different Mn contents at applied pressure of 1.8 GPa as compared in Tables 1 and 2. The $T_{MR}$ temperature increases strongly with increasing pressure, namely, by about 10 K in ceramics and by 41, 19, and 13 K in the film samples with $x = 0$, 0.1, and 0.2, respectively. From Figs. 1 and 2, it is apparent that above $T_{MD}(H)$ the $\rho(P = \text{const}, H)$ dependences are almost independent of magnetic field and are functions of only temperature and pressure.

In comparing the pressure and magnetic-field effects on the electrical properties of the ceramic and film manganites studied, one should note the following. The pressure and field effects on both the resistance and metal–insulator transition temperature are qualitatively similar, namely, they decrease the $\rho(H, P)$ values and increase $T_{MD}$. As a result, the ferromagnetic metallic phase is expanded. The $T_{MD}(P)$, $T_{MD}(H)$, and $T_{MR}(H)$ dependences are practically linear. The activation energy decreases as a function of both pressure and magnetic field (Table 4). Assuming the polaronic mechanism of conductivity in the films in the high-temperature phase, the decrease in activation energy can be explained as a reduced local relaxation around the more quickly hopping electrons. It leads to both a reduced high-temperature resistance and a lower magnetoresistance peak. The observed increase in transition temperature is a consequence of a hoping-induced destabilization of a polaronic phase.

Note that the magnetic-field effect on resistance decreases under pressure. In field $H = 8$ kOe, the fall in resistance is by about 11% and ~ 6% at $P = 0$ and 1.8 GPa, respectively. The change of the $T_{MD}$ temperature with magnetic field, $(\Delta T_{MD}/(H)$, is practically independent of pressure, and $(dT_{MD}/dP)$ coefficient is practically independent of magnetic field (Table 3). Unlike the pressure and magnetic-field effects on resistance and $T_{MD}$, their influence on MRE is opposite, namely, a magnetic field increases the MRE, while pressure decreases it. As a result of simultaneous influence of pressure and magnetic field the MRE decreases in both ceramics and the films (Table 2). This manifests itself more strongly in the films as well as with increasing pressure. However, while the suppression of spin fluctuations is the origin of the negative MRE in the films, the MRE in the ceramics is dominated by transport across grain boundaries [7].

The $T_{MR}$ temperature increases with increasing both pressure and magnetic field. The pressure and field effect on MRE is practically constant in ceramics and increases in the films as a manganese content increases.

The main mechanism responsible for the change of transport properties in manganites studied under pressure and in magnetic field is suggested to be related to the change of DE interaction between multivalent ions. The possibility to explain the pressure and field effects in the framework of DE model is due to the small residual resistance (of the order of or less than 1 mΩ·cm, as shown in Table 4) in the samples studied.

The pressure and magnetic-field effects on the metal–insulator transition and MRE are caused by an increase in both the effective electron transfer integral $t_{\text{eff}}$ and the mobility of charge carriers. However, the mechanisms of increase of $t_{\text{eff}}$ are different.

The pressure-induced reduction of both the unit cell volume and the lattice distortion results in the increase of the electron conductivity bandwidth, $W$, which is controlled by both the Mn–O distance and Mn–O–Mn bond angle. The applied pressure causes the average inclination angle of the $MnO_6$ octahedron to decrease and thus modifies both the length and angle of the bond. Under pressure the Mn–O–Mn angle opens toward 180°, increasing $t_0$ and, consequently, the strength of the DE interaction, which is determined by the transfer integral $t_{\text{eff}}$. The increasing electronic hopping amplitude favors an increase of both the conductivity and the phase transition temperatures.

The contraction of the unit cell volume at pressure increases an overlapping of the $3d(Mn^{3+})$–$2p(O^{2-})$–$3d(Mn^{4+})$ electron orbitals that also improves the effectiveness of the double exchange. As a consequence, this provides the shift of the metal–insulator transition (as well as the Curie temperature) towards higher temperatures expanding the ferromagnetic metallic phase in these manganites. Note, that the samples studied having higher $T_{MD}$, i.e., broader bandwidth, are less sensitive to pressure than those with lower $T_{MD}$.

According to the DE model, where a ferromagnetic interaction manifests itself by electrons transferred in narrow $e_g$ bands, the magnetic-field effect on the transfer of electrons between neighboring Mn sites is proportional to $\cos(\theta_{ij}/2)$. The ferromagnetic spin arrangement at $T < T_C$ reduces the randomness of the transfer. Along with temperature an external magnetic field forces the localized $t_{2g}$ spins to align parallel and hence reduces $e_g$ electrons scattering. A de-

crease of the angle between the two ionic states $\theta_{ij}$ favors the charge transfer and enhances the transfer integral $t_{\text{eff}}$. As a result the $T_{MD}$ temperature increases and the resistance decreases. Thus the magnetoresistance occurs mainly due to the Mn spins alignment by an applied magnetic field.

Based on published theoretical results [25], a quantitative estimation of the electron $e_g$ bandwidth and mean concentration $n$ per site of itinerant electrons was performed. A some modification taking into account a quantum spin fluctuations of itinerant $e_g$ electrons on the $Mn^{4+}$ ions bounded by the strong Hund interaction was carried out. The detailed analysis of the results will be published elsewhere.

In brief, the calculation performed is based on the perturbation method (PM), where the parameter of smallness is $1/z$ ($z$ is the nearest neighbour number of the $Mn^{4+}$ ion). The PM method differs from the coherent potential method (CPA) [38], wherein the contribution of spin fluctuations is overestimated. The specific resistance $\rho(n) = 1/\sigma(n)$, where $\sigma(n)$ is the conductivity, was calculated using the Kubo formula in simplest bubble approximation for pure double exchange [38]. Supposing that at $T = 0$ the contribution of electron–phonon interaction to the resistance is very small, one can write the following expression for the conductivity:

$$\sigma(n) = \frac{2\pi e^2}{3a\hbar} \int d\varepsilon\, \varepsilon D_c(\varepsilon)\varphi(\varepsilon, n)\,, \qquad (3)$$

where

$$\frac{d\varphi(t(\mathbf{q}), n)}{dt(\mathbf{q})} = A_{\mathbf{q}}(\mu, n)^2,$$

$A_{\mathbf{q}}(\mu, n)$ is the electron spectral density, which takes into account scattering of electrons and corresponds to noncoherent spectrum of excitations,

$$D_c(\varepsilon) = \frac{1}{N} \sum_{\mathbf{q}} \delta\left(\varepsilon - \frac{t(\mathbf{q})}{2t}\right)$$

is the electron density of states for the sc lattice, which does not take into account scattering of electrons and corresponds to coherent excitations, $t(q) = 2t \times$ $\times (\cos(q_x a) + \cos(q_y a) + \cos(q_z a))$ is the Fourier component of the hopping integral, $t$, with the $a$ is the lattice constant, $\delta$ is the Dirac delta function, $\varepsilon$ is the energy in $2t$ units, $N$ is the number of crystal lattice sites, $q_i$ is the projection of wave vector $q$ on the $i$ direction, $e$ is the electron charge.

The concentration dependence of residual resistance $\rho(n)$ calculated using the above method for ferromagnetic phase is presented in Fig. 6. The striking peculiarity is that, unlike the CPA where the minimal $\rho$ value is of the order of 1 mΩ·cm, in our case $\rho(n)$ tends to minimal value of order 0.012 mΩ·cm at

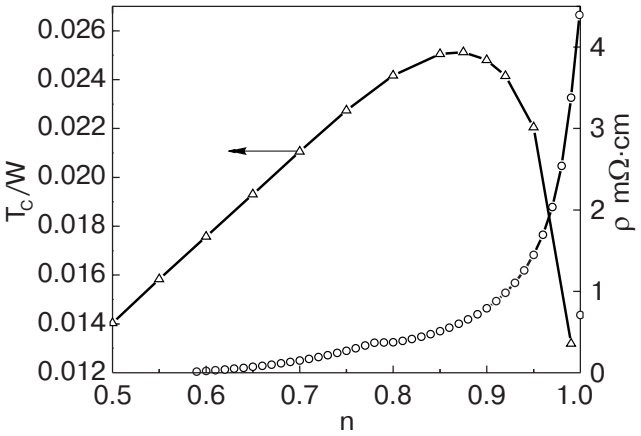


*Fig. 6.* Calculated critical temperature $T_C$ in $W$ units (left ordinate axis) and residual specific resistance $\rho$ (right ordinate axis) as a function of electron concentration $n$.

charge carriers concentration of $n \sim 0.59$. The calculated value corresponds to residual resistance for low $T$ observed experimentally in manganites studied (Table 4). Using the experimental $\rho_0$ values and theoretical $\rho(n)$ dependence, the electron concentration $n$ for the film LCMO, LCM1O, and LCM2O compounds was calculated at $P = 0$ and 1.8 GPa.

The temperatures $T_{MD}$ and $T_C$ are supposed to coincide. The following expression for critical temperature $T_C$ in $W$ units is the result of the performed previouusly analysis [43]:

$$T_C/W = \frac{768(\mu/W)^2 D_c\left(\frac{48\mu/W}{5-n}\right)}{(5-n)^3 + 384(\mu/W)(5-n)D_c\left(\frac{48\mu/W}{5-n}\right)}, \qquad (4)$$

where $\mu$ is the chemical potential.

Substituting $n$ calculated and experimental values of $T_{MD}$ in Eq. (4), we find the bandwidth values (Table 5). The phase transition temperature, $T_C/W$, as a function of $n$ is illustrated in Fig. 6. It should be noted that the calculated $W$ values (order of 1 eV) agree with results obtained in other works [2,11]. Experiments under pressure reveal a positive $dW/dP$ in the films (Table 5). The decreasing $dW/dP$ as $x$ increases is in agreement with changes of $dT_{MD}/dP$ (Table 3).

Table 5. Concentration of free charge carriers ($n_{\text{el}}$) and the electron conductivity bandwidth ($W$) in the films with different manganese content as a function of pressure (GPa).

| | LCMO | | LCM1O | | LCM2O | |
|---|---|---|---|---|---|---|
| | $P = 0$ | $P = 1.8$ | $P = 0$ | $P = 1.8$ | $P = 0$ | $P = 0.9$ |
| $n_{\text{el}}$ | 0.90 | 0.86 | 0.84 | 0.82 | 0.74 | 0.73 |
| $W$, eV | 0.83 | 0.95 | 0.92 | 0.98 | 1.04 | 1.09 |

Note that the weaker superexchange interactions (responsible for the antiferromagnetism) will also increases with pressure. However, the ferromagnetic DE interactions are stronger pressure dependent, since a pressure changes not only the unit cell parameters, but increases both the effective $e_g$ transfer integral and the charge carriers mobility as well.

## 4. Conclusions

In this work, a comparison of the transport properties of ceramic and film samples of manganites having the general formula $(La_{0.7}Ca_{0.3})_{1-x}Mn_{1+x}O_{3-y}$ ($x$ = 0–0.2) as a function of pressure, magnetic field, and manganese content has been performed.

The pressure—magnetic-field effects on resistance and MRE increase with increasing manganese content as a result of increase of the charge carriers density characterized by the $Mn^{4+}/Mn^{3+}$ ratio. According to the above experimental data, the pressure and magnetic field effects on the resistance and metal—insulator transition temperature are qualitatively similar in the two kind of samples, but differ quantitatively. The $T_{MD}$ temperatures are established to increase much stronger in the films than in ceramics with increasing pressure, magnetic field and manganese content. The pressure and magnetic-field effects on MRE are opposite: MRE decreases at applied pressure and increases with magnetic field. As a result of simultaneous influence of pressure and magnetic field the MR effect decreases in both ceramics and the films. MRE is shown to increase as a manganese content increases. The different pressure effects on resistance, MRE, and $T_{MD}$ in ceramic and film samples are connected with both granular structure of ceramics and difference of the oxygen nonstoichiometry in ceramic and film samples of the same content as well as with the film strain induced by lattice mismatch between the film and the substrate.

The main mechanism responsible for pressure and magnetic-field effects is related to the double exchange interaction. A magnetic field aligns the localized $t_{2g}$ spins, decreasing the angle $\theta_{ij}$ between the two ionic states and increases the charge carrier mobility; that leads to increasing $t_{\text{eff}}$ , which is proportional to $\cos(\theta_{ij}/2)$. This effect is responsible for the main part of the CMR. Unlike the films, where the MR effect is related to the reduction of spin fluctuations by an applied magnetic field, a large negative MR in ceramics is associated with magnetic domain rotation at the grain boundaries as well as with the tunneling effects. The pressure decreases the unit cell volume as well as the lattice distortion increasing the Mn–O–Mn bond angle ($\varphi$). As a consequence, the $e_g$ bandwidth and the transfer integral, proportional to $\cos(\pi - \varphi)$, increase; that is favorable to an increase of the DE interaction in the Mn–O network. The pressure effect can be also interpreted as a result of an overlapping of the $3d(Mn^{3+})$–$2p(O^{2-})$–$3d(Mn^{4+})$ electron orbitals at the contraction of the unit cell volume that also improves conditions of the double exchange. A various theoretical models (VRH, Mott and Holstein laws) were used for the analysis of $\rho(T, P, H)$ dependences at $T > T_{MD}$ and $T < T_{MD}$. In an attempt to find the best theoretical fit to the experiment, we have tested each approximation for the minimal root-mean-square deviation of the experimental and calculated points. A calculation of the residual resistance in the structure with short-range magnetic order caused by scattering on spin fluctuations was also performed. The phase transition temperature was determined taking into account the quantum fluctuation of electron spin. The results of calculation were used to determinate both the concentration of free charge carriers and the electron conductivity bandwidth as well as their changes under pressure in the films with various manganese content. A comparison of the calculation and experimental data shows that there is a direct correlation between $T_{MD}$ and $W$ and between MRE and $n$ at applied pressure, namely, the increasing metal–insulator temperature follows the increasing electron conductivity bandwidth and the decreasing magnetoresistance effect correlates with the decreasing concentration of charge carriers.

This work was in part supported by the Polish Government Agency KBN (Project 1 P03B 025 26) and by the Russian Foundation for Basic Research (Grant No. 04-02-17598). V.I. Mikhaylov thanks the MIANOWSKI FUND for the financial support. The help offered by Mgr. S. Kucherenko during realization of this work is gratefully acknowledged.

1. A.P. Ramirez, *J. Phys.: Condens. Matter*. **9**, 8171 (1997).
2. J.M.D. Coey, M. Viret, and S. von Molnar, *Adv. Phys.* **48**, 167 (1999).
3. C. Zener, *Phys. Rev*. **81**, 403 (1951).
4. P.-G. de Gennes, *Phys. Rev*. **118**, 141 (1960).
5. S. Tamura, *J. Magn. Magn. Mater*. **31–34**, 805 (1988).
6. Y. Moritomo, A. Asamitsu, and Y. Tokura, *Phys. Rev*. **B51**, 16491 (1995).
7. H.Y. Hwang, T.T.M. Palstra, S.-W. Cheong, and B. Batlog, *Phys. Rev*. **B52**, 15046 (1995).
8. Z. Arnold, K. Kamenev, M.R. Ibarra, P.A. Algarabel, C. Marquina, J. Blasko, and J. Garcia, *Appl. Phys. Lett*. **67**, 2875 (1995).
9. J.J. Neumeier, M.F. Hundley, J.D. Thompson, and R.H. Heffner, *Phys. Rev*. **B52**, R7006 (1995).
10. J.M. De Teresa, M.R. Ibarra, J. Blasko, J. Garcia, C. Marquina, P.A. Algarabel, Z. Arnold, K. Kamenev, C.

Ritter, and R. von Helmolt, *Phys. Rev.* **B54**, 1187 (1996).
11. V. Laukhin, J. Fontcuberta, J.L. Garcia-Munoz, and X. Obrados, *Phys. Rev.* **B56**, R10009 (1997).
12. A. Nossov, J. Pierre, J. Beille, V. Vassiliev, and B. Slobodin, *Eur. Phys. J.* **B6**, 467 (1998).
13. J.S. Zhou and J.B. Goodenough, *Phys. Rev. Lett.* **62**, 3834 (2000).
14. V.E. Arkhipov, V.S. Gaviko, K.M. Demchuk, V.P. Diakona, A.V. Kovalev, Ya.M. Mukovski, E.A. Nejfeld, and R.V. Pomortsev, *Pisma JETF* **71**, 169 (2000).
15. I.V. Medvedeva, K. Berner, G.H. Rao, N. Hamad, Yu.S. Bersenev, and J.R. Sun, *Physica* **B292**, 250 (2000).
16. Y.S. Wang, A.K. Heilman, B. Lorenz, Y.Y. Xue, C.W. Chu, J.P. Frank, and W.M. Chen, *Phys. Rev.* **B60**, R14998 (1999).
17. V. Markovich, E. Rozenberg, A.I. Shames, G. Gorodesky, I. Fita, K. Suzuki, R. Puzniak, D.A. Shulyatev, and Ya.M. Mukovski, *Phys. Rev.* **B65**, 144402 (2002).
18. J.S. Zhou, W. Archibald, and J.B. Goodenough, *Nature* **381**, 770 (1996).
19. J. Fontcuberta, V. Laukhin, and X. Obrados, *Appl. Phys. Lett.* **72**, 2607 (1998).
20. T. Roch, S. Yaghoubzadeh, F.S. Razavi, B. Leibold, R. Praus, and H.-U. Habermeier, *Appl. Phys.: Mater. Sci. Process.* **A67**, 723 (1998).
21. V. Moshnyaga, S. Klimm, E. Gommert, R. Tidecka, S. Hom, and K. Samwer, *J. Appl. Phys.* **88**, 5305 (2000).
22. G.M. Gross, R.B. Praus, S. Yaghoubzadeh, F.S. Razavi, and H.-U. Habermeier, *J. Alloys and Comp.* **317-318**, 141 (2001).
23. S.S. Kucherenko, V.I. Mikhaylov, V.P. Pashchenko, P.I. Polyakov, V.A. Shtaba, and V.P. Dyakonov, *Pisma JTF* **27**, 38 (2001).
24. V. Dyakonov, I. Fita, E. Zubov, V. Pashchenko, V. Mikhaylov, M. Arciszewska, Yu. Bukhantsev, W. Dobrowolski, A. Nabialek, and H. Szymczak, *J. Magn. Magn. Mater.* **246**, 40 (2002).
25. E. Zubov, V.P. Dyakonov, and H. Szymczak, *JETF* **122**, 1044 (2002).
26. V. Dyakonov, V. Shapovalov, E. Zubov, P. Aleshkevych, A. Klimov, V. Varyukhin, V. Pashchenko, V. Kamenev, V. Mikhaylov, K. Dyakonov, V. Popov, S.J. Lewandowski, M. Berkowski, R. Zuberek, A. Szewczyk, and H. Szymczak, *J. Appl. Phys.* **93**, 2100 (2003).
27. W. Bazela, V. Dyakonov, V. Pashchenko, B. Penc, H. Szymczak, J.H. Hernandez-Velasco, and A. Szytula, *Phys. Status Solidi* **B236**, 458 (2003).
28. V. Dyakonov, V. Pashchenko, E. Zubov, V. Mikhaylov, Yu. Bukhantsev, I. Fita, V. Turchenko, N.A. Doroshenko, A. Szewczyk, R. Zuberek, and H. Szymczak, *Phys. Solid State* **45**, 914 (2003).
29. V.P. Pashchenko, A.A. Andreev, A.A. Shemyakov, V.K. Prokopenko, E.G. Darovskikh, O.P. Cherenkov, and A.D. Loiko, *Neorg. Mater.* **34**, 62 (1998).
30. C. Ritter, M.R. Ibarra, J.M. De Teresa, P.A. Algarabele, C. Marguina, J. Blasko, J. Garcia, S. Oseroff, and S.-W. Cheong, *Phys. Rev.* **B56**, 8902 (2000).
31. H.L. Ju and M.K. Kannan, *Solid State Commun.* **104**, 419 (1997).
32. J.R. Sun, H.W. Yeung, H. Li, K. Zhao, H.N. Chan, and H.K. Wong, *J. Appl. Phys.* **90**, 2831 (2001).
33. N. Abdelmoula, K. Guigare, A. Cheikh-Rouhou, E. Dhahvi, and J.C. Joubert, *J. Solid State Chem.* **151**, 139 (2000).
34. L. Friedman and T. Holstein, *Ann. Phys.* (N.Y.) **21**, 494 (1963).
35. T. Holstein, *Ann. Phys.* (N.Y.) **8**, 325 (1959).
36. G. Jakob, W. Westerburg, F. Martin, and H. Adrian, *Phys. Rev.* **B58**, 14966 (1998).
37. M. Viret, L. Ranno, and J.M.D. Coey, *Phys. Rev.* **B55**, 8067 (1997).
38. D.M. Edwards, A.C.M. Green, and K. Kubo, *J. Phys.: Condens. Matter.* **11**, 2791 (1999).
39. A.J. Millis, R. Mueller, and B.I. Shraiman, *Phys. Rev.* **B54**, 5405 (1996).
40. M.B. Salamon and M. Jaime, *Rev. Mod. Phys.* **73**, 583 (2001).
41. M. Jaime, P. Lin, M.B. Salamon, and P.D. Han, *Phys. Rev.* **B58**, R5901 (1998).
42. P. Shiffer, A.P. Ramirez, W. Bao, and S.-W. Cheong, *Phys. Rev.* **B75**, 3336 (1995).
43. E. Zubov and V.P. Dyakonov, *Cond.-Mat.* 0509370.